Electrochemical immunosensor based on Al-TCPP nanomaterial adsorption aggregation signal amplification for the detection of dengue virus NS1 protein

zixuan zhang
Chongqing Medical University
wei li
Chongqing Medical University
jie liu
Chongqing Medical University
ying li
Chongqing Medical University
chaorui li (crli@cqmu.edu.cn)
Chongqing Medical University

Research Article

Keywords: Dengue virus NS1, Al-TCPP/MB, Electrochemistry, Adsorption, Electrochemical immunosensor

Posted Date: May 30th, 2023

DOI: https://doi.org/10.21203/rs.3.rs-2970406/v1

Abstract

To detect the dengue virus NS1 protein with high sensitivity, this research suggests an electrochemical immunosensor based on the Al-TCPP adsorption aggregation signal amplification approach. We created a type of metal-organic framework (MOF) material called astrophytum myriostigma, which resembles a cactus plant and has a large specific surface area. Additionally, it can produce electrostatic attraction with the amino groups on methylene blue (MB), firmly fix MB on the MOF material, and manage MB reunion after adsorption, which is helpful for electron transmission and amplifies the electrical signal. The cationic dye methylene blue has redox characteristics. It possesses a high electron transfer rate, electrochemical reversibility, and strong biocompatibility. The generated electrochemical immunosensor has good reproducibility and stability, and the relationship between the analyte concentration and electrical signal strength is linear. The suggested immunosensor has a broad detection range from 10 fg/mL to 100 ng/mL with a low detection limit of 9.12 fg/ml under ideal conditions.

1. Introduction

Due to its potential to lead to serious illnesses such as dengue hemorrhagic fever (DHF) and dengue shock syndrome, dengue is one of the most dangerous diseases for humans[1, 2]. The current report stated that the dengue virus kills thousands of people every year and is the main cause of serious disease and death in approximately 112 nations[3]. Four main serotypes of dengue, DENV-1, DENV-2, DENV-3, and DENV-4, are indigenous to tropical and subtropical regions, but they are currently spreading to other higher latitudes throughout the world[4]. Although there is still no specific vaccination, there are precise therapeutic methods available depending on the severity of the condition. Therefore, to prevent patients from contracting life-threatening infections, early identification and treatment may be crucial[5].

Additionally, dengue patients may collect flavivirus NS1, a glycoprotein and crucial immunogen that is produced in the circulation by infected cells, at levels as high as 50 ng/mL[6]. Early in the course of the infection, high amounts of NS1 are discovered in the sera of DENV-infected individuals, and there is evidence linking NS1 to DHF development. Hemorrhage, coagulopathy, and a significant increase in vascular permeability are the primary features that distinguish DHF from the more benign forms of the illness. High levels of circulating NS1 in sera correlate with disease severity and risk of progression to DHF[7]. This manuscript focuses on the highly conserved 43–48 kDa glycoprotein known as the dengue NS1 protein. Presently, it is utilized as a substantial diagnostic biomarker of infection starting on the first day following the onset of illness, in contrast to IgM, which is often detectable after 4–6 days [2]

Currently, a number of analytical techniques have been used, such as virus isolation and cultivation followed by an immune fluorescence assay[8], a window for virus cultivation, reverse-transcription polymerase chain reaction (RT—PCR) detection of RNA[8], and monoclonal antibody capture-enzyme-linked immunosorbent assay (MAC-ELISA)[9]. However, some techniques lack enough sensitivity, some may innately rely on pricey apparatus, and some include difficult and time-consuming steps such as purification, preconcentration, and conventional isolation procedures[10, 11]. Therefore, it is necessary to

create NS1 determination techniques that are quick, accurate, selective, and inexpensive. Due to their high sensitivity, mobility, low cost, noninvasive nature, ultrafast detection, and miniaturisability, electrochemical immunosensor devices have attracted much research attention in this field for the detection of tiny analytes. Sensitive and accurate biomarker identification at the appropriate moment is necessary for rationalized infectious disease therapy. [12, 13]. The immunosensing transducer in particular is very selective because of its extraordinary selectivity between the antigen and antibody, which potentially makes it appropriate for medical diagnostics.

Due to their exceptional photophysical and electrochemical capabilities, porphyrins and porphyrin derivatives have garnered considerable interest in the domains of catalysis, biosensing, gas storage, solar cells, and medicinal applications[14]. However, several intrinsic constraints, including self-quenching, weak absorption in the biological spectrum window, and poor chemical and optical stability, significantly restrict their biological applicability, particularly in the therapy and diagnostics of cancer. To overcome the drawbacks of porphyrins and enable their use in biomedicine, a new family of hybrid porous coordination polymers called porphyrin-based metal-organic frameworks has been created. Metal ions, metal clusters, and porphyrin ligands are used in the self-assembly of porphyrin-based MOFs. Porphyrin-based MOFs can be changed or loaded with functional molecules or pharmaceuticals to provide therapeutic and imaging capabilities while still maintaining the unique features of porphyrins[15]. Porphyrin-based MOFs combine the benefits of porphyrin materials and metal-organic frameworks. Porphyrin-based 2D MOFs (MTCPP, M = Zn, Cu, Co, Ni) were created by Yao et al. for mixed matrix membranes to improve the performance of organic solvent nanofiltration[16]. To significantly increase the catalytic capacity and conductivity of nonenzymatic amplification, Dong et al. invented two-dimensional (2D) ultrathin Cu-TCPP(Fe) nanosheets with a large surface area that can be made available for many active sites. These nanosheets also provide modified active sites for antibody immobilization as signal tags[17]. Unfortunately, porphyrin-based MOF materials are rarely employed in electrochemical immunosensors owing to their high porosity and adsorption aggregation. Therefore, Al-TCPP, which has a large specific surface area, excellent biocompatibility, and outstanding adsorption capabilities for a variety of colors, is synthesized in this work.

The redox cationic dye mediator of phenothiazines includes methylene blue (MB). It possesses strong biocompatibility, a high electron transfer rate, and electrochemical reversibility. [18]. It has several uses in electrochemical biosensors as an electron transfer medium that is also in charge of electron production and signal amplification[19, 20]. The sensitivity of the sensor is increased by the Ab-Au@SiO_2-MB signal tag, which was made of MB nanodots and an Au@SiO_2 carrier loaded with antibodies. This is because of the strong EC signal of the MB nanodots and the high differential labeling between the detection Ab and MB signal probes[17]. However, MB is very water-soluble. The nonspecificity and low stability of MB in the conventional homogenous electrochemical sensing system may unavoidably skew the diagnostic outcomes. [20].

Al-TCPP, a porphyrin metal derivative that resembles a cactus plant and is known as Astrophytum myriostigma. Al-TCPP/MB-Ab_2 was also created as a signal tag by combining the benefits of the high

porosity of MOF material, and it was used to adsorb and stabilize MB, which significantly decreased its dissolution in water. Al-TCPP and MB are able to produce powerful electrostatic attraction as well. It might successfully stop the MB signal from leaking during the test. Additionally, the adsorption of Al-TCPP, which was advantageous for the transmission of electrons, can accelerate MB agglomeration [21]. The experiment demonstrated good performance in the detection of dengue virus NS1 protein in genuine sample serum and had good stability, selectivity, and repeatability, offering a workable strategy for clinical NS1 detection.

2. Experimental methods

2.1 Reagents

Unless otherwise stated, all commercial compounds were purchased without additional purification. Both cetyltrimethylammonium bromide (CTAB) and aluminum (III) chloride hexahydrate (AlCl36H2O, AR) were purchased from Sigma—Aldrich. Shanghai Census Biotech provided the tetrakis (4-carboxyphenyl) porphyrin (TCPP, 97%) that was purchased. Sinopharm Chemical Reagent Co. Ltd. was the source for the N, N-dimethylformamide (DMF, > 99.5%), and ethanol (C2H5 OH, > 99.5%) that were acquired. The antigens and antibodies for dengue virus NS1 were purchased from Maiyue Biotechnology Co., Ltd. Phosphate-buffered hydrochloric acid (PBS, pH = 6.8) containing 0.1 M Na_2HPO_4, 0.1 M KH_2PO_4, and 0.1 M KCl was used as a working buffer for the electrochemical measurements. All other reagents were of analytical grade and were not further purified. Ultra-pure distilled and deionized water (18.2 MΩ) obtained from the MilliporeMill-Q purification system was used throughout the experiments as all solution preparations.

2.2 Apparatus

All electrochemical measurements, including cyclic voltammetry (CV), chronoamperometry (i-t), constant potential deposition, and electrochemical ac impedance spectroscopy (EIS), were performed on an AUTO LAB PGSTAT302 N electrochemical workstation with a three-electrode system. The three-electrode system consisted of Ag/AgCl (containing 3 M KCl) as the reference electrode, a platinum wire electrode as the counter electrode, and a modified glassy carbon electrode (GCE, 3 mm diameter) as the working electrode. Scanning electron microscopy (SEM) and energy dispersive spectrometry (EDS) image acquisition were performed using a Hitachi SU8020 (Hita chi Limited Japan). Zeta analysis was performed by a Zetasizer Nano ZS90. A High-Speed Automated Surface Area and Pore Size Analyzer (ASAP 2460 micromeritics). Fourier transform infrared spectrometer (Nicolet IS10 Thermo Nicolet Corporation) (FTIR-850).

2.3 Preparation of Al-TCPP

Synthetically produced Al-TCPP nanosheets were made with the use of surfactants. Deionized water was added to TCPP (200 mg, 0.223 mmol), AlCl36H2O (150 mg, 0.621 mmol), and CTAB (100 mg) (25 mL). At room temperature, the suspension was sonicated for 10 minutes. The combined solution was then put

into a 100 mL Teflon-line autoclave and heated for 16 hours at 180°C. To remove unreacted components and attached CTAB molecules, the mixture was centrifuged at 8000 rpm for 5 minutes before being washed twice with DMF (2×20 mL) and twice with acetone (2×40 mL)[22].

2.4 Preparation of Al-TCPP/MB

In a 50 mL beaker, 20 mL of ultrapure water was added, and the pH was then adjusted to 8.0 using NaOH and HCl. Next, 0.05 g of Al-TCPP and 0.025 g of MB were weighed and added, along with a magnet. The beaker was then left to stand for 6 h before being stirred again. Any MB that was not securely adsorbed was removed by centrifuging the solution and washing it six times with ultrapure water. The centrifuged material was dried in a vacuum drying oven at 50°C overnight. The Al-TCPP/MB material was subsequently produced effectively.

2.5 Preparation of the immunosensor

2.5.1 Preparation of secondary antibody label Al-TCPP/MB-Ab_2 (NS1)

To disperse 4 mg of Al-TCPP/MB material, 1 mL of ultrapure water was added, followed by the addition of 1 mL of the NS1 secondary antibody (Ab_2) and magnetic stirring for 12 hours. The non-specificity of the unlinked material site was then blocked by adding 300 mL of 1 wt% BSA and stirring for two hours.

2.5.2 Assembly process of immunosensor

First, 3 mm diameter glassy carbon electrodes were polished with 0.3 μm and 0.05 μm alumina suspensions, cleaned repeatedly by ultrasonication in alternating baths of ultrapure water and anhydrous ethanol, and dried under nitrogen. The electrode was then used to deposit gold nanoparticles (Au NPs) twice, each time for 30 seconds, onto the surface of the glassy carbon electrode. After that, deionized water was used to wash the primary antibody that was not linked to the electrode after adding 8 μL of primary antibody (Ab_1) drop by drop. Ab_1 was then added and incubated at 4°C for 12 hours. To block nonspecific connection sites, 8 μL 1 wt% BSA was added dropwise and incubated at 4°C for 1 h. Deionized water was then used to rinse the ligated BSA that was not connected. The unattached ligated BSA was then rinsed with deionized water. Drop by drop, 10 μL of various antigen concentrations (NS1) were then added. These were then incubated at 45°C for 70 minutes before the disconnected NS1 was washed away. After 1 hour of incubation at 37°C with 8 μL of secondary antibody label (Al-TCPP/MB-Ab_2) was added dropwise, the disconnected Al-TCPP/MB-Ab_2 was removed by washing. Using a three-electrode system, testing was conducted in a 5 mM $[Fe(CN)_6]^{3-/4-}$solution containing 0.1 M KCl at pH = 7.0 (DPV). The voltage range of the tests was from − 0.2 V to 0.6 V. The fabrication process of the immunosensor is shown in Scheme 1.

2.5.3 Detection of NS1

By using cyclic voltammetry (CV) and electrochemical impedance spectroscopy (EIS) in a solution of 5 mmol/L $[Fe(CN)_6]^{3-/4-}$ containing 0.1 mol/L KCl, it was possible to characterize the working electrode preparation process. Next, the DPV signal was tested in the same solution at a potential of -0.2 V to 0.6 V and a scanning rate of 50 mV/s. The choice of potassium ferrocyanide as the buffer solution for this DPV experiment was inspired by a patent for a magnetic molecular-imprinting sensor for the detection of Gram-negative bacteria signaling molecules[23].

3 Results and discussion

3.1 Material characterization of Al-TCPP

As shown in Fig. 1a, Al-TCPP-MOFs, which are extremely porous and stable aluminum-based porphyrinic MOFs, were created by the hydrothermal reaction of $AlCl_3 \cdot 6H_2O$ and H_2TCPP at 180°C. In the reaction system, porphyrin linkers join infinite $Al(OH)O_4$ chains to form a 2D microporous framework. The Al-TCPP MOFs have the potential to be employed as an adsorption material because of their porous and insulating properties.

The morphology of the material was characterized by transmission electron microscopy. As shown in Fig. 1b, it is a translucent polygonal body. There is a connecting edge in the middle that looks like a top view of the astrophytum myriostigma. There were many pores, which provided sites for the adsorption of methylene blue. It can also be seen from the scanning diagram in Fig. 1c that the material does look like a plant in the cactus family, which is called astrophytum myriostigma, and it has a large specific surface area.

The effectiveness of MB adsorption is significantly influenced by the porosity of Al-TCPP. Al-TCPP and its nanosheets' true accessible volume were calculated using isothermal N_2 sorption assays carried out at 77 K to ascertain their porous characteristics[24]. Through the test, the nitrogen adsorption isotherm diagram is obtained, as shown in Fig. 1d. The complete hysteresis loop that results from the nonoverlapping adsorption and desorption isotherms, which is more consistent with type IV adsorption isotherm features, demonstrates that the pores inside Al-TCPP materials are primarily tiny holes[25]. The specific surface area is 451.38 m^2/g, Al-TCPP/MB, and it is fitted by the BET model appropriate for mesoporous materials. Since only MB is adsorbed, the difference in the specific surface area indicates that Al-TCPP adsorbs a significant quantity of MB. Nonlocal density functional theory (NLDFT) is utilized as a calculation model to simulate the pore size distribution of the Al-TCPP material. The result is presented in Fig. 1e, and the pore size is primarily dispersed between 2 and 8 nm. This indicates that Al-TCPP has a large specific surface area, rich pores, and strong adsorption.

3.2 Adsorption amplification mechanism of Al-TCPP/MB

Zeta potential is significant because the stability of colloidal dispersion is correlated with its value. The strength of the mutual attraction or repulsion between particles is measured by the zeta potential. The

system is more stable, and dissolution or dispersion can resist aggregation; the smaller the molecule or dispersed particle is, the greater the absolute value (positive or negative) of the zeta potential[21]. It should be noted that the absolute value of the Zeta potential represents its stability, and the positive and negative values represent what kind of charge the particle takes. On the other hand, the lower the Zeta potential (positive or negative), the more likely it is to condense or condense, which means that the attraction outweighs the repulsive force, the dispersion is destroyed, and condensation or condensation occurs[26]. Zeta potential analysis of Al-TCPP, Al-TCPP/MB, and MB solutions are shown in Fig. 2a and **b**. The result that the positively and negatively charged MB complexes react to reduce the solutions' Zeta potential electronic configuration demonstrates that the Al-TCPP/MB complexes' primary method of action is electrostatic adsorption of positive and negative charges between ions.

The Al-TCPP adsorption of MB is due to electrostatic attraction as the dominant force. In Fig. 2c, according to the Fourier infrared spectroscopy (FTIR) of Al-TCPP, the carboxylate groups of TCPP are mostly associated with Al^{3+} in MOFs, as evidenced by the fact that Al-carbonyl TCPP's (C = O) stretching of -COOH at 1680 cm^{-1} is significantly damped when compared to that of the TCPP ligand. The stretching and in-plane vibration modes of -NH in the freebase porphyrin rings are represented by peaks at 3310 cm^{-1} and 960 cm^{-1} respectively[22]. The curve where Al-TCPP adsorbs MB is curve c. The hydroxyl peak may be seen at 3500 – 3300 cm^{-1}, the amino peak at 1650 – 1590 cm^{-1}, and the amide bond peak at 1531 – 290 cm^{-1}. The amino peak can be seen at 1650 – 1590 cm^{-1}, and the b line represents the spectrum of MB[27]. Since MB is a cationic dye in electrostatic adsorption (pKa = 5.85), when the pH of the solution containing MB exceeds pKa, the H on the MB will be removed from the solution as H^+. The MB cation and carboxylate anion on the adsorbent becomes more positive in charge due to this [28].

Moreover, we used electrochemical characterization to verify the signal amplification effect of Al-TCPP/MB. It can be seen from Fig. 2d that Al-TCPP itself does not generate an electrical signal. A powerful electrical signal will be produced at a potential of 0.1 V once the MB has been absorbed. This result means that a large amount of MB was absorbed by Al-TCPP, moreover, MB can help Al-TCPP to generate stronger current signals; and appear oxidation peaks in 5 mmol/L $[Fe(CN)_6]^{3-/4-}$ buffer.

3.3 CV and EIS characterization of the immunosensor assembly process

The preparation process of the working electrode was characterized by CV and EIS. The results are shown in Fig. 3a and Fig. 3b. Figure 3a is the CV of the electrode modification process. After performing the CV test on the electrode's bare surface (Curve a), the Au NPs were placed at a voltage of -0.2 V (Curve b). The antigen (Curve e) was linked, Al-TCPP/MB-Ab_2 was connected, the nonspecific site was blocked with 1 weight percent BSA, and finally, Ab_1 (Curve c) (Curve f) was connected. Finally, the figure shows that the conductivity drops gradually from c to f because both antigens and antibodies are biological macromolecular proteins, it's going to block electron transfer. As a result of the protein's layer-by-layer

attachment to the electrode, the electrode's resistance steadily rises. The impedance diagram in Fig. 3b also verifies this result. In Fig. 3b, each curve corresponds to the curve in Fig. 3a; the larger the radius of the semicircle corresponding to each line is, the larger the impedance is, and the radius of lines c to f increases successively, which also proves that the electrode assembly is successful.

3.4 Conditional optimization of immunosensor

The pH of $[Fe(CN)_6]^{3-/4-}$, incubation duration, incubation temperature, and secondary antibody label concentration were all tuned to achieve sensitive detection of NS1. These factors have a strong influence on the immunosensor system. The immunosensor's analytical performance is significantly influenced by the pH of PBS. On the one hand, the pH level influences the protein's affinity for the conductive substance. Strong acidity or alkalinity, on the other hand, might result in protein denaturation. Figure 4a shows that the sensor functioned best when the secondary antibody label's Al-TCPP/MB concentration was 10 μg/mL. The concentration of the dropped antigen and the antigen's incubation period both had an impact on the amount of antigen that adhered. It can be seen from Fig. 4b that the antigen (NS1) incubation time was optimal at 70 min. The antigen may not be connected if the time was too short, and the activity of the antigen will decrease if it is too long. As shown in Fig. 4c, the optimal binding temperature of antigen and antibody is 35 ℃. If the binding temperature is too high, it will easily lead to protein denaturation and inactivation, and if the temperature is too low, it may inhibit protein activity. Therefore, the incubation temperature of 35 ℃ is the best. Figure 4d shows the optimal pH condition optimization of the immunosensor. It can be seen from Fig. 4d that the signal of the sensor was the strongest when pH = 7.0, indicating that the sensor had the best performance when pH = 7.0.

3.5 Immunosensor linearity test

The assay was incubated at various concentrations under ideal detection conditions before DPV tests were run. As shown in Fig. 5a, as the assay concentration rose, the magnitude of the signal grew as well. A linear correlation was present, and the detection range was between 10 fg/mL and 100 ng/mL. The detection limit was 9.12 fg/mL (S/N = 3), and the correlation equation was $I = 132.4964 + 23.29\ C_{NS1}$ (R^2 = 0.99819). I (A) is the immunosensor's response current, and C (ng/mL) is the analyte's concentration. The findings demonstrated that the sensor has a high NS1 detection limit and a broad detection range.

3.6 Reproducibility, selectivity, and stability of the immunosensor

Figure 6a shows the selective analysis of different antigens (HgIg, AFP, H-FABP, Mix) by the sensor. It can be seen from the figure that the sensor has almost no signal response to HgIg, AFP, H-FABP, and Mix but only responds to NS1. This result showed that the sensor had good selectivity. Figure 6b shows the reproducibility test of the sensor. Five immunosensors were created and detected at the same level of NS1 (10 pg/mL). Additionally, the relative standard deviation (RSD) of the five immunosensor

measurements was 2.39%, indicating that the immunosensor showed acceptable repeatability. Figure 6C shows the stability test of the immunosensor. The modified electrodes were tested for stability using chronoamperometry every five days while being kept in a sealed container at 4°C. In comparison to the original current signal, the average of five parallel current signals only declines by 4.8% after 20 days (Fig. 6c), indicating high stability.

3.7 Application of immunosensor in serum sample

We analyzed serum samples with known NS1 concentrations and then added various quantities of NS1 to the samples to further examine the immunosensor's performance. The immunosensor recovered NS1 with a range of 97.81–100.42% and an RSD of 0.13–3.26% (Table 1). These results show that the immunosensor can be successfully applied for the clinical detection of NS1.

Table 1
Recovery results of the immunosensor in serum samples in 5 mmol/L $[Fe(CN)_6]^{3-/4-}$) solution containing 0.1 mol/L KCl solution (n = 5).

Sample	The addition content (ng/mL)	The av value (ng/mL)	RSD (%, N = 5)	Recovery (%)
1	0.1	0.1076	3.26	97.81%
2	1	1.0142	1.4	100.42%
3	10	10.0028	0.13	99.93%

4. Conclusion

Al-TCPP adsorption of MB was employed in this experiment as a novel adsorption aggregate signal amplification technique for NS1 detection in an electrochemical immunosensor. Al-TCPP was developed as a MOF material with excellent adsorption capabilities, and it has a surface area of 451.38 m^2/g. Methylene blue signal leakage during testing may be efficiently stopped by it. The regulation of MB reunion after adsorption by Al-TCPP is advantageous for electron transmission. The created electrochemical immunosensor offers superior consistency and sensitivity when compared to earlier detection techniques. The suggested immunosensor displayed a broad detection range from 10 fg/mL to 100 ng/mL under ideal circumstances, with a low detection limit of 9.12 fg/mL (Table 2).

Table 2
Comparison of the present immunosensor with other reported NS1-based dengue biosensors.

Number	Type of sensor	Method	Linear range (ng/mL)	LOD (ng/mL)	Ref
1	SPGE surface-modified AuNPs–PEG–Ab–TEMPO	CV	0-1000	50	[29]
2	Antibody-Ag NPs as trace tag using sandwich-type immunosensor using Pencil graphite electrode	DPV	3-300	0.5	[30]
3	Dual marker label-free electrochemical assay	EIS, CV	1-5000	0.340	[31]
4	Al-TCPP/MB aggregation signal amplification strategy	DPV	$1*10^{-6}$-100	$9.12*10^{-6}$	This work

Declarations

Ethical Approval:

The ethical review number for human serum is 2020-542.

Competing interest:

The authors declare that they have no known competing financial interests or personal relationships that could have appeared to influence the work reported in this paper.

Authors' contributions:

Zixuan zhang wrote the main manuscript text; Jie liu and Yin li, Wei li reviewed the manuscript, Chaorui li is our teacher who gave us many help.

Funding:

This work was supported by the Natural Science Foundation of Chongqing, China (No. cstc2019jcyj-msxmX0121).

Availability of date and materials:

Not applicable.

References

1. M. H. Nawaz, A. Hayat, G. Catanante, U. Latif, and J. L. Marty, Anal Chim Acta **1026**, 1 (2018).
2. A. Dhal, T. Kalyani, S. Ghorai, N. K. Sahu, and S. K. Jana, Sensors International **1**, (2020).

3. S. S. Hegde and B. R. Bhat, Biosens Bioelectron X **10**, (2022).
4. J. H. Amorim, R. P. dos S. Alves, S. B. Boscardin, and L. C. de S. Ferreira, Virus Res **181**, 53 (2014).
5. A. C. M. S. Dias, S. L. R. Gomes-Filho, M. M. S. Silva, and R. F. Dutra, Biosens Bioelectron **44**, 216 (2013).
6. M. R. de Lima and R. Bresaola, Revista DAE **58**, 4 (2010).
7. A. C. Alcalá, F. Medina, A. González-Robles, L. Salazar-Villatoro, R. J. Fragoso-Soriano, C. Vásquez, M. Cervantes-Salazar, R. M. del Angel, and J. E. Ludert, Virology **488**, 278 (2016).
8. O. Parkash and R. H. Shueb, Viruses **7**, 5410 (2015).
9. F. S. R. R. Teles, Anal Chim Acta **687**, 28 (2011).
10. J. Ruta, S. Rudaz, D. v. McCalley, J. L. Veuthey, and D. Guillarme, J Chromatogr A **1217**, 8230 (2010).
11. Z. Yu, T. Kabashima, C. Tang, T. Shibata, K. Kitazato, N. Kobayashi, M. K. Lee, and M. Kai, Anal Biochem **397**, 197 (2010).
12. L. L. Liu, L. Marques, R. Correia, S. P. Morgan, S. W. Lee, P. Tighe, L. Fairclough, and S. Korposh, Sens Actuators B Chem **271**, 24 (2018).
13. F. Mollarasouli, S. Kurbanoglu, and S. A. Ozkan, Biosensors (Basel) **9**, (2019).
14. N. Rabiee, M. T. Yaraki, S. M. Garakani, S. M. Garakani, S. Ahmadi, A. Lajevardi, M. Bagherzadeh, M. Rabiee, L. Tayebi, M. Tahriri, and M. R. Hamblin, Biomaterials **232**, (2020).
15. Z. Wang, Q. Sun, B. Liu, Y. Kuang, A. Gulzar, F. He, S. Gai, P. Yang, and J. Lin, Coord Chem Rev **439**, (2021).
16. A. Yao, D. Hua, F. Zhao, D. Zheng, J. Pan, Y. Hong, Y. Liu, X. Rao, S. Zhou, and G. Zhan, Sep Purif Technol **282**, (2022).
17. L. Dong, L. Yin, G. Tian, Y. Wang, H. Pei, Q. Wu, W. Cheng, S. Ding, and Q. Xia, Sens Actuators B Chem **308**, (2020).
18. J. Li, Q. Wang, L. Zheng, and H. Liu, J Mater Sci Technol **41**, 68 (2020).
19. S. Bu, K. Wang, Z. Li, C. Wang, Z. Hao, W. Liu, and J. Wan, Analyst **145**, 4328 (2020).
20. F. Mollarasouli, K. Asadpour-Zeynali, S. Campuzano, P. Yáñez-Sedeño, and J. M. Pingarrón, Electrochim Acta **246**, 303 (2017).
21. P. P. Gopmandal and J. F. L. Duval, Curr Opin Colloid Interface Sci **60**, 101605 (2022).
22. H. Yu, X. Wu, Q. Mu, Z. Wei, Y. Gu, X. Yuan, Y. Lu, Z. Deng, and Y. Peng, Chinese Chemical Letters **32**, 3833 (2021).
23. (n.d.).
24. T. Zelenka, Microporous and Mesoporous Materials **227**, 202 (2016).
25. A. Ramírez, L. Sierra, M. Mesa, and J. Restrepo, Chem Eng Sci **60**, 4702 (2005).
26. M. Manciu, F. S. Manciu, and E. Ruckenstein, Adv Colloid Interface Sci **244**, 90 (2017).
27. S. Y. Wang, L. F. Fang, and H. Matsuyama, Langmuir **35**, 9152 (2019).

28. Z. Jiaqi, D. Yimin, L. Danyang, W. Shengyun, Z. Liling, and Z. Yi, Colloids Surf A Physicochem Eng Asp **572**, 58 (2019).
29. P. D. Sinawang, L. Fajs, K. Elouarzaki, J. Nugraha, and R. S. Marks, Sens Actuators B Chem **259**, 354 (2018).
30. M. Awan, S. Rauf, A. Abbas, M. H. Nawaz, C. Yang, S. A. Shahid, N. Amin, and A. Hayat, J Mol Liq **317**, (2020).
31. A. Santos, P. R. Bueno, and J. J. Davis, Biosens Bioelectron **100**, 519 (2018).

Scheme 1

Scheme 1 is available in the Supplementary Files section.

Figures

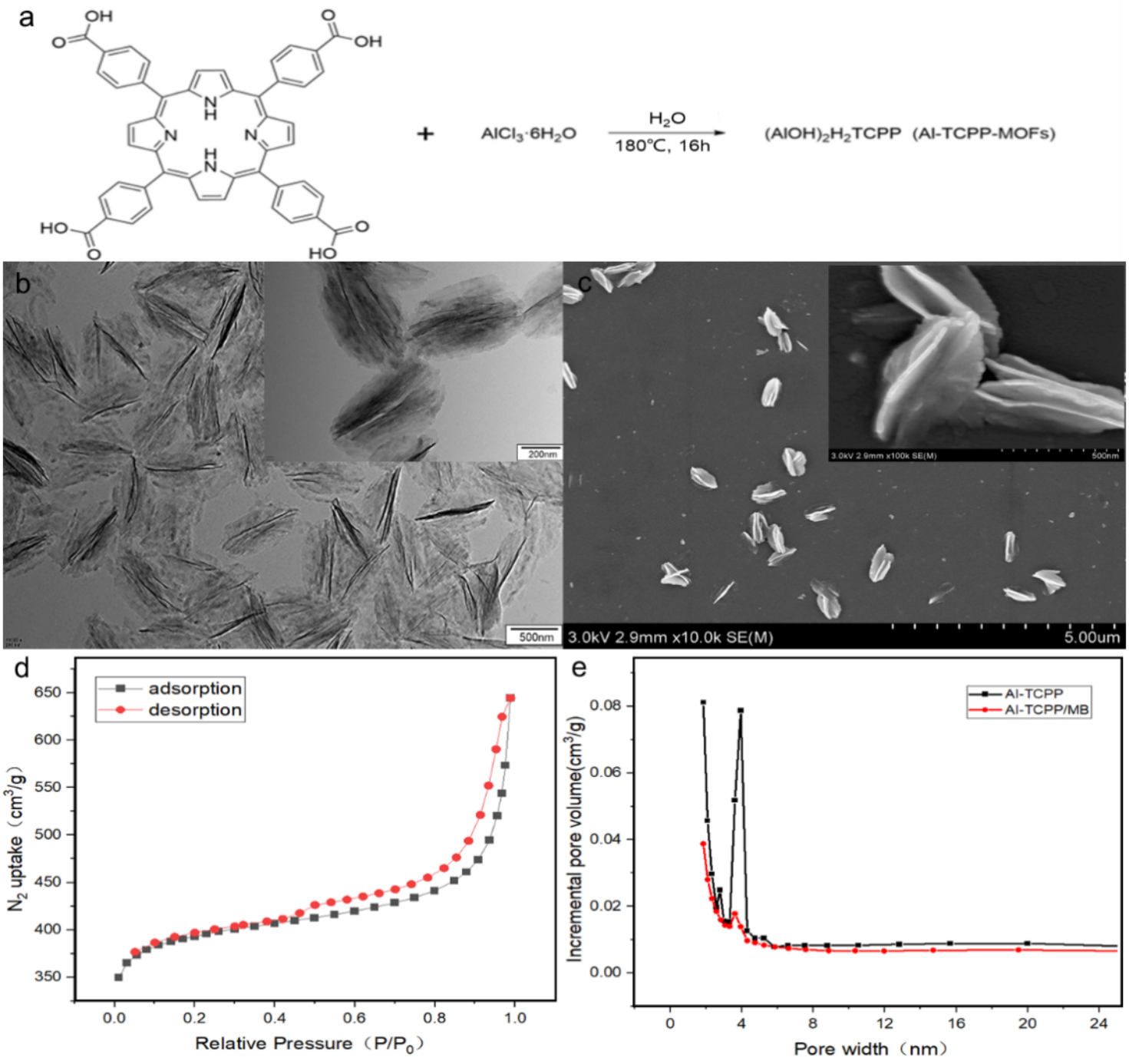

Figure 1

(a) The diagrammatic flow chart of Al-TCPP-MOFs (b/c) TEM and SEM characterization of MOF-235 scanning electron microscope (d) Nitrogen adsorption and desorption isotherm (e) Al-TCPP and Al-TCPP/MB pore size distribution

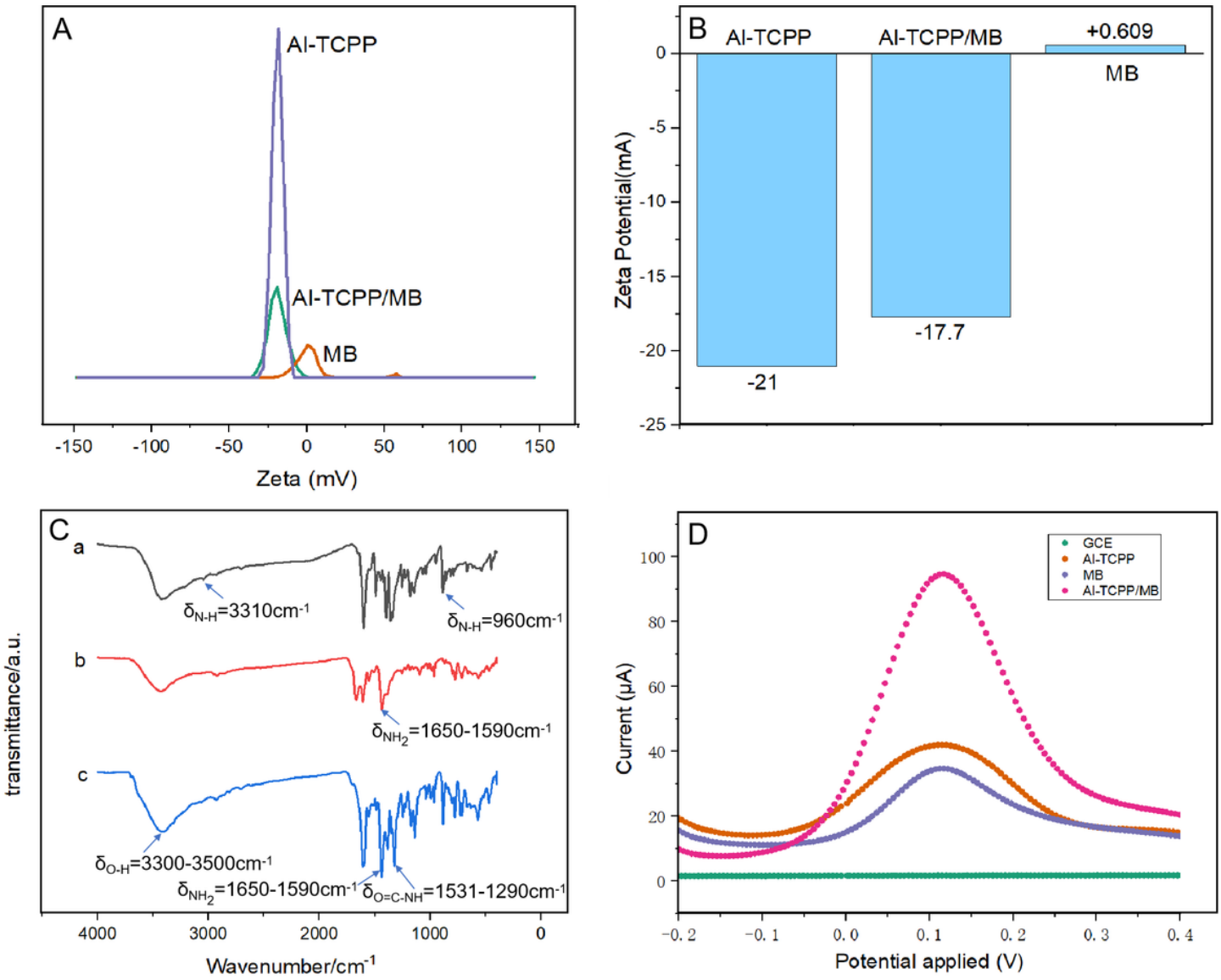

Figure 2

(a/b) Zeta potential of Al-TCPP Al-TCPP/MB and MB (c) FTIR spectrum of the synthesized Al-TCPP (a) MB (b) Al-TCPP/MB (c) (d) Signal comparison between Al-TCPP adsorbed and unadsorbed MB DPV (C_{NS1}= 0.1 ng/mL)

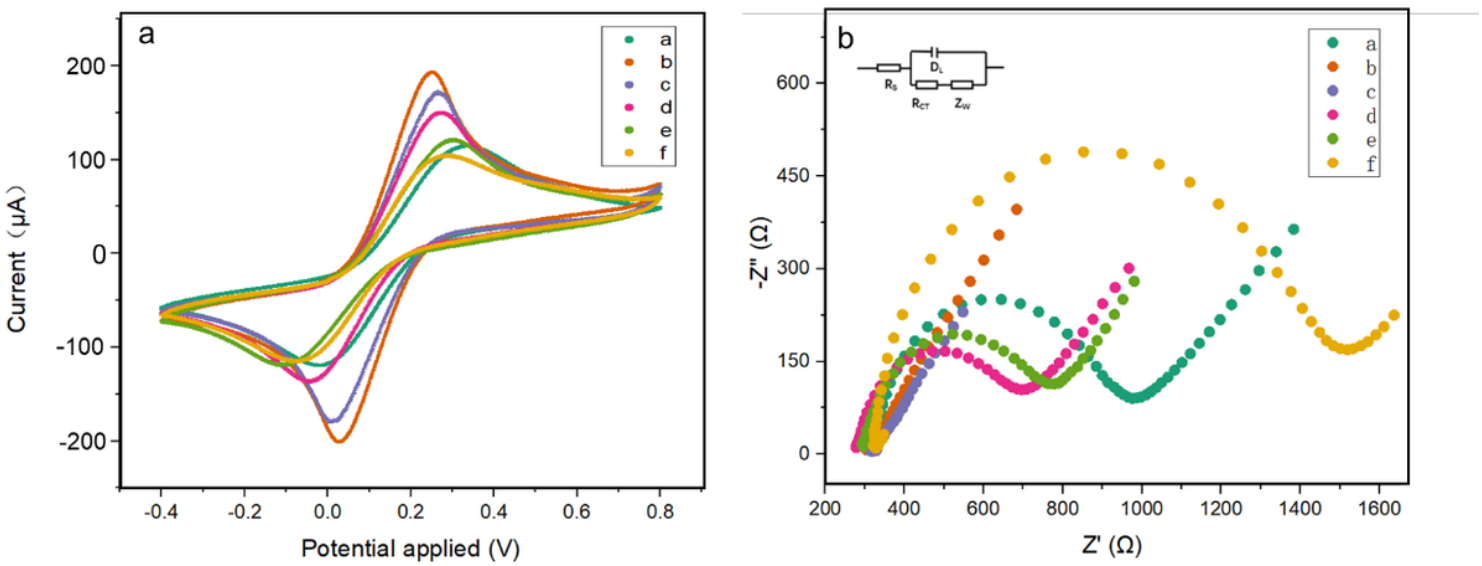

Figure 3

(a) CV and (b) EIS of the immunosensor assembly process: a→f: GCE, Au/GCE, Ab_1/Au/GCE, BSA/Ab_1/Au/GCE, NS1/Ab_1/Au/GCE, Ab_2-Al-TCPP/MB/NS1/BSA/Ab_1/Au/GCE

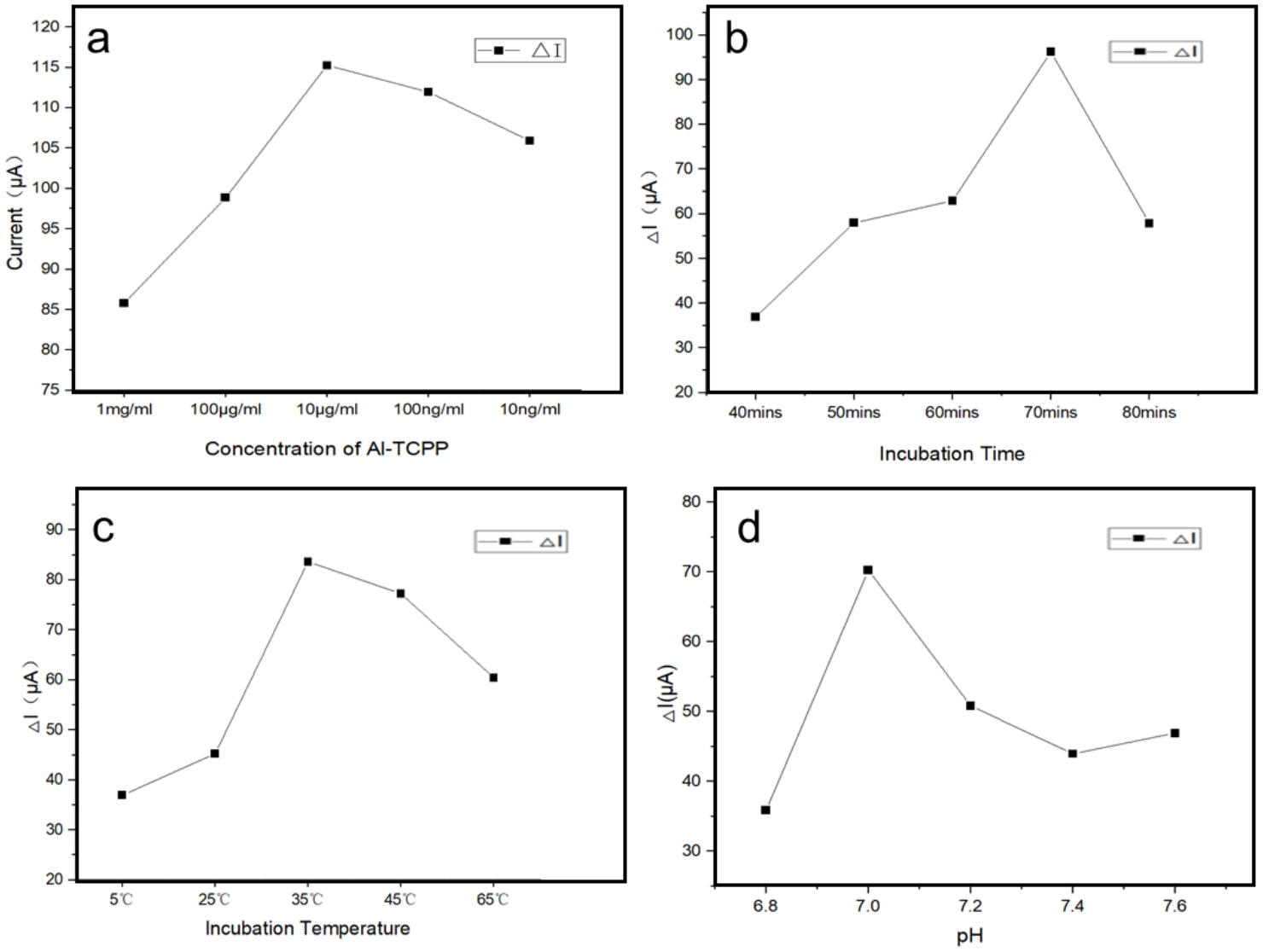

Figure 4

Optimization of experimental conditions: (a) concentration of Al-TCPP, (b) incubation time, (c) antigen antibody binding time, and (d) pH

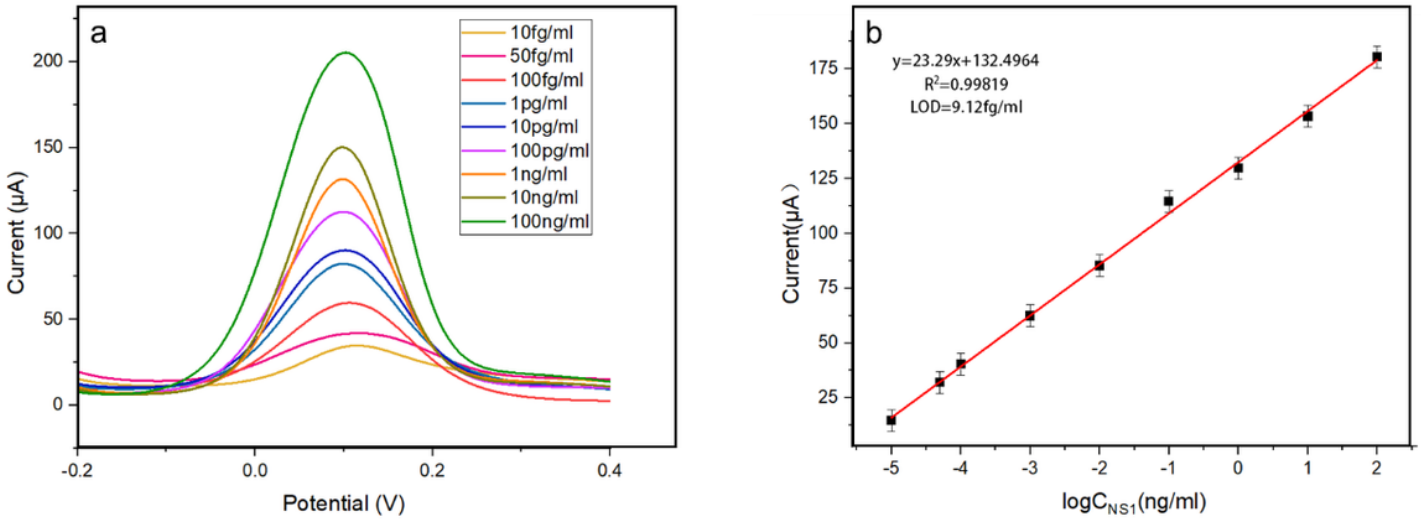

Figure 5

(a) DPV of electrochemical immunosensors with different NS1 concentrations (b) Calibration curve of the immunosensor for the detection of different concentrations of NS1

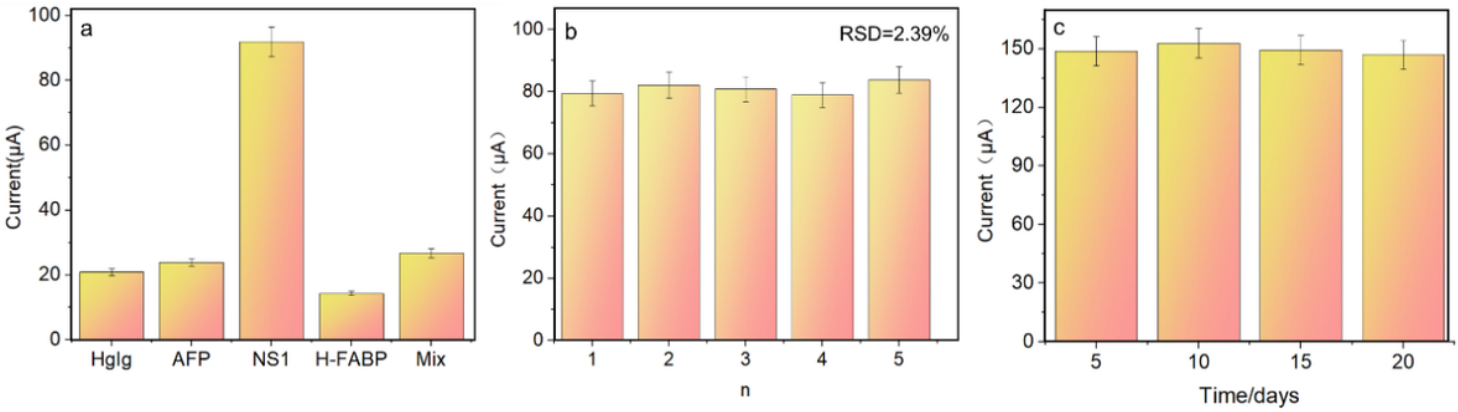

Figure 6

(a) Selective test of the sensor (C_{NS1} = 10 pg/mL C(HgIg AFP H-FABP Mix) = 20 ng/mL) (b) Reproducibility of 5 different electrodes modified with 10 pg/ml NS1 (c) stability test of the Sensor within 20 days (C_{NS1} = 10 ng/mL)

Supplementary Files

This is a list of supplementary files associated with this preprint. Click to download.

- Scheme1.png